The Response of Geopotential Height Anomalies to El Niño and La Niña Conditions and Their Implications to Seasonal Rainfall Variability over the Horn of Africa

Solomon Gunta[1], Hejamady Gangadhara Bhat[2], Busnur Rachotappa Manjunatha[2]

[1]Department of Physics, College of Natural and Computational Sciences, Wolaita Sodo University, Wolaita Sodo, Ethiopia
[2]Remote Sensing and Geo-Informatics Division, Department of Marine Geology, Faculty of Science and Technology, Mangalore University, Karnataka, India
Email: solgunta@gmail.com, gangadharrbhat@gmail.com, manjzircon@gmail.com

Abstract

In this study, we unveil atmospheric circulation anomalies associated with the large-scale tropical teleconnections using National Center for Environmental Prediction (NCEP) reanalysis dataset. Composite analyses have been performed to know the impact of large-scale tropical circulations on the Horn of Africa. The composite analysis performed at the geopotential height of 850 Mb and 200 Mb, and precipitation rate (mm/day) during six strong El Niño and La Niña episodes revealed that the large-scale tropical variability induced climate anomalies in space and time. A substantial decrease in upper-level height (200 Mb) has been observed in the study area during El Niño composite years as compared to the La Niña years. During El Niño conditions, the upper-level divergence initiates low-level vertical motion, thereby enhancing convection, however, during La Niña composite years, nearly contrasting situations are noticed in Belg (February to May) season in Ethiopia. However, geopotential height anomalies at 850 Mb are above-normal during the strong El Niño years, suggesting suppressed convection due to vertical shrinking and enhancement of divergence at the lower level. Compared to the Belg (February to May), geopotential anomalies were generally positive during the Kiremt (June to September) season, thereby suppressing the rainfall, particularly in Southern Ethiopia and Northern Part of Kenya. In contrast, an increase in rainfall was observed during the Belg season (February to May).

Keywords

Geopotential Height, Composite Analysis, ENSO, Atmospheric Circulations, NCEP Reanalysis, Tropical SST Anomalies, Teleconnections, Belg, Kiremt

1. Introduction

The climate variability at any regional level is predominantly controlled by lower and upper-level atmospheric circulations which in turn are prominently mediated by the nearby and distant Oceanic thermal responses. Likewise, the climate in the Horn of Africa (HOA) varies from arid to tropical monsoon conditions due to the seasonal modulation of upper and lower atmospheric circulation patterns triggered by teleconnection forces [1]. Different scientific reports documented that the climate variability across the HOA and Eastern equatorial Africa (EEA) is mainly influenced by the large-scale seasonal atmospheric circulation as well as the warm waters of the Indian and Pacific Ocean [1] [2]. Besides season climate variations, the climate of the region varies over a much longer period. Internal and external forcing of the climate system results in Decadal and longer-term variability in the climate system [3] [4] [5]. [1] [6] further noted that, on the centennial, multi-decadal, and decadal time, the main mode of climate variability is observed in the Atlantic, Indian, Pacific, and the Southern Ocean and they result in a significant influence on regional as well as global atmospheric circulation.

According to [7], tropical large-scale circulation features dominating the Horn of Africa (HOA) are mainly controlled by a continent-ocean temperature gradient, a seasonal reversal of winds caused by the hemispheric scale circulations driven by convections in tropical oceans and complex topographic orientations in the region. Different studies uncovered the upper and lower level atmospheric circulation patterns are associated with seasonal rainfall variability over the HOA during the dominant rainy seasons [8] [9] [10] [11] [12]. The recent study that investigated changes in the mean state of rainfall over East Africa asserted that rainfall in the region exhibits considerable variability across spatial and temporal extent and this variability is caused by the complex interactions between different large scale atmospheric and oceanic features acting at regional and global scales [13]. Sea Surface Temperature in the equatorial Pacific Ocean is characterized by ENSO (El Niño Southern Oscillation) episodes [10]. Even though the equatorial Pacific Ocean are distant from the HOA, they are significantly correlated with climate variations (temperature, rainfall, upper and lower level circulation patterns, humidity, etc.) over the region, however, the extent and sign of correlations and seasonality are not uniform across the region [14] [15] [16].

Owing to topographic complexity in the region, the northern Ethiopia high lands and northwestern parts of the HOA have boreal summer monsoon from June to September (JJAS) locally known as "Kiremt" and it accounts for 50% to 80% of the annual rainfall over the region [16] [17]. Whereas, the equatorial part of the Great Horn of Africa (GHA) has two rainy seasons, the long rainy season from March to May (MAM) and the short rainy season from October to December (OND) [17] [18]. A diagnostic study carried out by [19] on monsoon dynamics in the region verified that usually two distinct monsoons patterns are

observed near the HOA, which are known as Northeast (NE) and Southwest (SW) monsoons. As further notified by [19], the SE monsoons are observed during the Northern Hemisphere Summer (June-August), while the NE monsoons are dominant during Southern Hemisphere Summer (December-February). Yet, the transition in monsoonal wind occurs during the Northern Hemisphere Spring (March-May) locally known as a long-rainy season and characterized by convergence in the Equatorial Africa Region (EEA) when low-level air masses move from both NE and SE meet and form a zone of convergence in the region. The model study performed at the regional level also captured observed circulation anomaly patterns, with divergence at the lower level and convergence at the upper level during rainfall deficit years, but for the wet years, divergence (convergence) was simulated at the upper (lower) level [20]. Similarly, the spatial and temporal variability of rainfall over Ethiopia during summer (JJAS), locally known as Kiremt, is well captured by the satellite-based observations and, model simulation data [21]. According to [21], most parts of the country are dominated by the intensity and position of upper Tropical Easterly Jet (TEJ), lower East Africa Low-Level Jet (EALLJ), and Westerly from the south Atlantic basin. The model, as well as observation-based studies, confirmed that strong/weak TEJ is associated with excess/deficit rainfall overall in Ethiopia, with the particular exception of the southern rim of the country [7] [19] [21] [22] [23].

In this study, we tried to explore the association between upper and lower level geopotential height anomalies and strong ENSO episodes during selected composite years, and observe enhanced/suppressed convective activities in response to the change in circulation pattern. Our study area encompasses the HOA with special reference to Ethiopia because due to its complex landscape nearly all types of climate zone in the region are observed in Ethiopia. The highly complex terrain features combined with the myriad synoptic systems that produce rainfall variability, has resulted in a very diverse climate that spans eight different climate zones that range from warm to humid highland climate, and Ethiopia encompasses seven of the eight climate zones in the region [24] [25]. This study was mainly focused on two seasons in Ethiopia locally known as Kiremt (June to September) and Belg (February-May). The study has attempted to discern the response of upper and lower geopotential height anomaly to ENSO phenomena on and associated seasonal modulation of precipitation patterns in the study area.

2. Study Area

The study area is shown in the rectangular black box in Figure 1; below encompasses Ethiopia, Somalia, Kenya, Uganda, Rwanda, Tanzania, and South and North Soudan partially [24] [26], however, our analysis more focused on Ethiopia due to most of the climate zones in the region found there. The region is known for its complex topographic features with the lowest part below sea level found in the north-Eastern part of Ethiopia (Denkel Depression) and Mount Kilimanjaro in Tanzania with 5895 m above sea level. According to [1], the equator
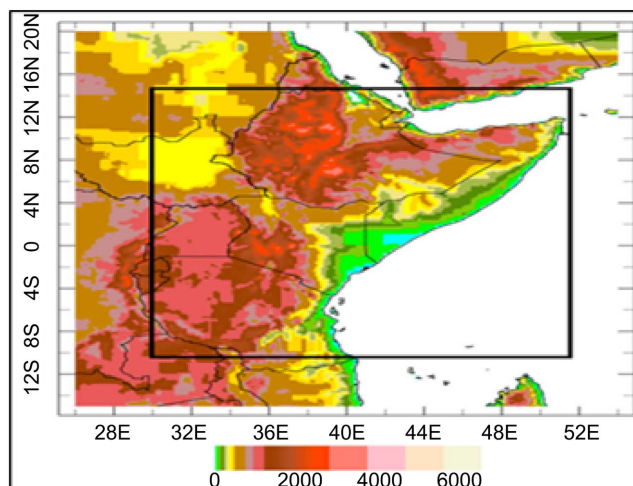
Figure 1. Map showing the topography (elevation in meters; Bradfield Lyon, 2014, International Research Institute for Climate and Society).

passes through Uganda, Kenya, and Somalia, so that above the equatorial line the northern part receives the majority of its rain during the boreal summer (June to September) while below the equator southern part receives the majority of its rain during the austral summer months (December to February). The region is influenced by the seasonal migration of the Inter-Tropical Convergent Zone (ITCZ) and results in four different rainfall seasons over the region: December-February, March-May, June-September, and October-December [1] [9] [24] [26] [27].

3. Data and Methodology

3.1. Data

The data from the National Center of Environmental Prediction (NCEP) reanalysis data set has been used by the climate diagnostic center (https://www.esrl.noaa.gov/psd/). [7] [28] pointed out that the reanalysis dataset was derived from historical observations that have been quality controlled and modeled with a modernized, fixed version of the NCEP global data assimilation system. As fully described in [29], the NCEP uses a frozen state-of-the-art global data assimilation system and a database complete as possible. They further noted that the reanalysis project involves, the recovery of the land surface, ship, rawinsonde, pibal, aircraft, satellite, and other data; quality controlling and assimilating these data with a data assimilation system that is kept unchanged over the reanalysis period 1957-96 [29]. This dataset has been used rigorously by numerous researchers to predict the weather, water, climate extremes and to further understand and diagnose the state of the climate system at regional as well as to the globe extent [7] [9] [11] [20] [23] [28] [29] [30]. We used, surface precipitation rate (mm/day), geopotential height at 850 Mb, and 200 Mb data from NCEP source, to monitor climate fluctuations in the study area that are caused by remote atmospheric and oceanic coupling. To avoid some inconsistent data,

we restricted our reanalysis data as much as possible to the era of meteorological satellites, our analysis is limited from 1981 to 2020.

3.2. Methodology

Composite analysis has been used to explore the relationship between temporal viabilities for precipitation rate (mm/day) and, upper and lower level geopotential height (Mb) in the study area to remote oceanic and atmospheric properties. The composite analysis involves identifying and averaging one or more categories of fields selected according to their linkage to key climate conditions [19]. Results of composites are then used to generate hypotheses for patterns that may be associated with the individual scenarios [20] [31]. The key conditions selected for this study are the strongest El Niño and La Niña years as mentioned in **Table 1**; the intensity of geopotential height and precipitation rates long-term mean, seasonal mean, and anomalies have been investigated across selected years.

According to Diro *et al.* [23], composite analysis has an advantage over individual case studies because compositing emphasizes commonly occurring features while smoothing more random fluctuations. The composite analysis is also better than correlation because it allows the study of non-linearity [23]. Different researchers have used the composite method over East Africa to investigate common features and patterns in climate variables [20] [32] [33] [34]. We adopted the same method to explore the anomalies patterns of geopotential height (850 Mb and 200 Mb) and precipitation rate (mm/day) associated with strong El Niño and La Niña episodes in selected composite years.

Composite Map has been generated to show long term mean averaged from 1981 to 2010, arithmetic means of composite years, and anomalies (departure from long term mean) for surface precipitation rate, geopotential height at 850 Mb and 200 Mb respectively to investigate the impact of El Niño and La Niña on the HOA region. The anomalies were calculated as the difference between the actual values of the selected meteorological variables and their long-term mean values in a specified composite period. We selected the six strongest El Niño and La Niña years for composite analysis. Only six years have been selected for composite analysis because including weaker events or using more than six events introduces

Table 1. Selected variables for composite analysis for strong El Niño and La Niña years

S. No	Strong El Niño Years	Strong La Niña Years	Variables selected of Composite Analysis
1	1982	1988	Surface precipitation Rate (mm/day)
2	1987	1995	
3	1994	1998	Geopotential height at 200 Mb
4	1997	1999	
5	2009	2007	Geopotential height at 850 Mb
6	2015	2010	

undesirable variability that tends to obscure important patterns, processes, and mechanisms [7].

The Oceanic Niño Index (ONI) has become the de-facto standard that NOAA uses for identifying El Niño (warm) and La Niña (cool) events in the tropical Pacific. It is the running 3-month mean SST anomaly for the Niño 3.4 region (*i.e.*, 5˚N - 5˚S, 120˚ - 170˚W). Events are defined as 5 consecutive overlapping 3-month periods at or above the +0.5˚ anomaly for warm (El Niño) events and at or below the −0.5˚ anomaly for cold (La Niña) events. The threshold is further broken down into Weak (with a 0.5 to 0.9 SST anomaly), Moderate (1.0 to 1.4), Strong (1.5 to 1.9), and Very Strong (≥2.0) events. The ENSO episodes to be categorized as weak, moderate, strong, or very strong must have equaled or exceeded the threshold for at least 3 consecutive overlapping 3-month periods (https://ggweather.com/enso/oni.htm).

4. Results and Dissections

4.1. Composite Analysis of Key Meteorological Variables

The previous studies carried out in the region, especially in Ethiopia revealed that the total rainfall amount was mainly contributed by Kiremt (JJAS) and Belg (FMAM), while the contribution of the driest season Bega (ONDJ) was insignificant [9]. Therefore, we employed a composite analysis of pertinent variables based on the two dominant seasons in the rainfall amount that most of the region depends on, to associate with the large-scale tropical drivers. As one can see from the composite maps shown below, clear contrasts have been observed for the two dominant rainfall seasons in the region. The composite maps presented below compare the long-term mean or climatology, composite means value, and composite anomalies of selected variables during the six strongest El Niño and La Niña years respectively.

4.2. Variations in Geopotential Height during the Strong El Niño Years

Previous studies done by various researchers explored that the climate of East Africa regions is strongly linked to the climate in the tropics through the upper and lower lever responses to the convection in the eastern and central Indian Ocean, Maritime continent, eastern and western Pacific Ocean [3] [7] [9] [10] [11] [13] [15] [26] [28] [35]. [28], noted that change in convection in the vicinity of the Maritime continent and western Pacific, through Rossby-Kelvin wave dynamics, can lead to changes in the upper-level circulation over southwest Asia and can be extended to the HOA.

According to [23], the effect of a warm equatorial eastern Pacific (El Niño) depends on the season of occurrence and the region of Ethiopia. Specifically, El Niño in the previous winter is associated with excess Kiremt (JJAS) rainfall, whereas El Niño in the contemporaneous summer is associated with deficit Kiremt rainfall except for the northwestern part of the country. They further no-

ticed that, for the northwest, El Niño is always associated with deficit rainfalls irrespective of the season of occurrence. This shows the response of large-scale features for different parts of the county is not merely similar due to terrain complexity [10] [12] [21] [26].

Geopotential height approximates the actual height of a pressure surface above mean sea level [36] [37] [38] [39]. Therefore, a geopotential height observation represents the height of the pressure surface above mean sea level. Geopotential height is valuable for locating troughs and ridges which are the upper-level counterparts of surface cyclones and anticyclones. As affirmed by various authors [35] [40], seasonal to annual rainfall variations in Ethiopia as well as the neighboring countries in the East Africa region, are associated with the macro-scale pressure systems developed in Indian and Atlantic Oceans and monsoon flows.

4.3. Geopotential Height at 850 Mb during the Strong El Niño Years

As one can see from **Figure 2**, below, clear contrast has been observed in the long-term mean, a composite mean, and the composite anomaly of geopotential
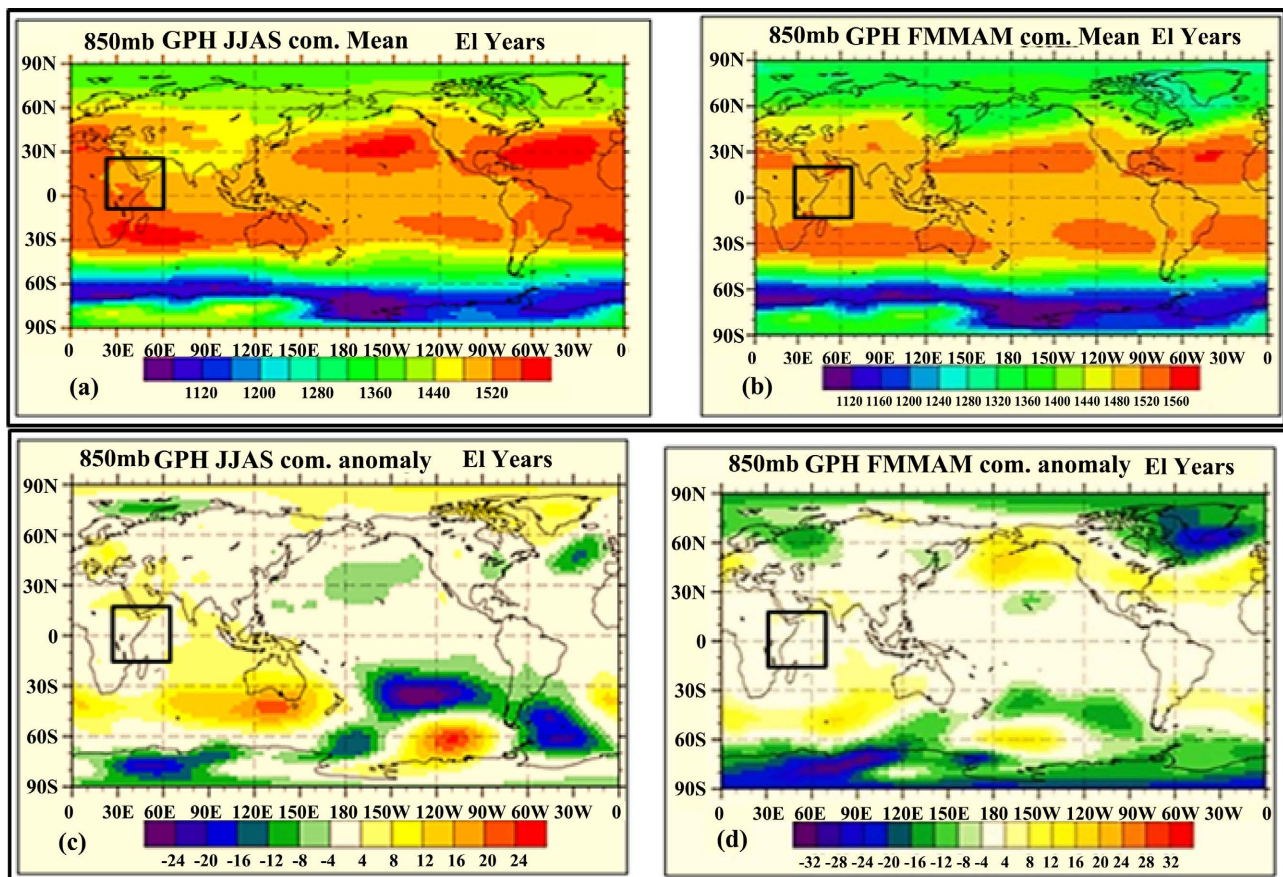

Figure 2. Geopotential heights (850 Mb, in meters) (a) JJAS composite Mean; (b) FMAM composite Mean; (c) JJAS composite Anomaly of six strongest El Niño events; (d) FMAM composite anomaly of six strongest El Niño events. NB: The rectangular inset box closely encompasses the study area (HOA).

height for JJAS and FMAM seasons during six-strong El Niño years selected for composite analysis. Above normal geopotential height at 850 Mb during El Niño years depict suppressed convections owing to vertical shrinking that enhance divergence at a low level and suppressed precipitation. More positive anomaly (see Figure 2(c) and Figure 2(d) in JJAS compared to FMAM shows, El Niño effects in Kiremt (JJAS) seasonal rainfall is more than contemporaneous Belg (FMAM) season. Also strongly contrasting convective activities observed in the southeastern Pacific and western Pacific during JJAS than FMAM and this results in relatively strong teleconnectivity between the tropical Pacific Ocean and Ethiopia height anomalies in JJAS than FMAM.

4.4. Geopotential Height at 200 Mb during the Strong El Niño Years

Regarding the upper-level height anomaly at 200 Mb, Figure 3(c) & Figure 3(d) shows fairly contrasting features with height anomaly at 850 Mb, particularly during the JJAS season. Associated with this, [28] depicted that, in the tropics, the response at the lower level is often the opposite of what is observed in the upper levels. The above normal height anomaly in the upper level is linked to
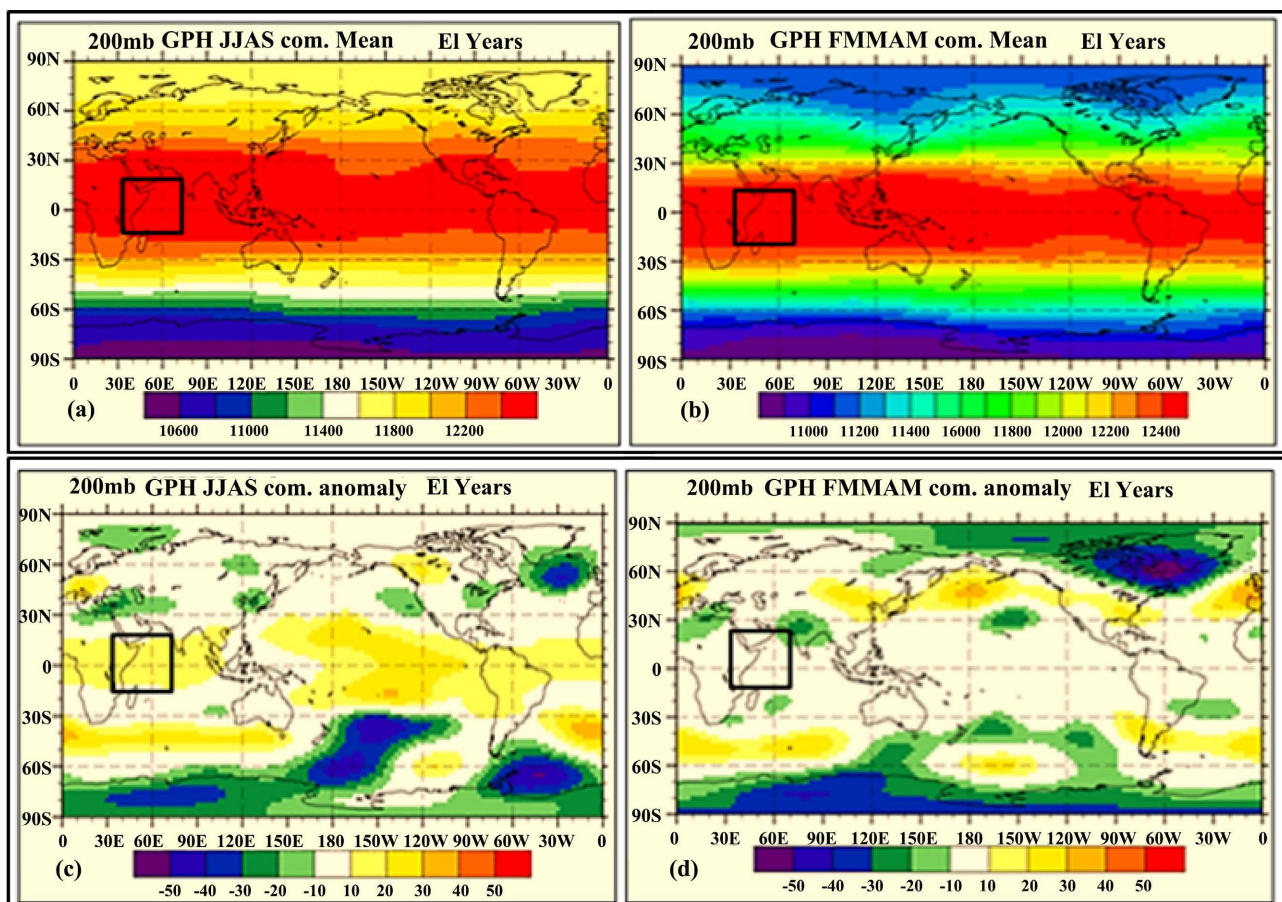

Figure 3. Geopotential heights (200 Mb, in meters) for (a) JJAS composite mean; (b) FMAM composite Mean; (c) JJAS composite Anomaly of six strongest El Niño events; (d) FMAM composite anomaly of six strongest EN events.

suppressed convection but below normal height, the anomaly is related to the enhanced convention.

According to [23], during the short rainy season in the northern highland of Ethiopia, the existence of a trough (low pressure) has been observed over the Red Sea at about 200 Mb height. This trough pattern corresponds to an anomalous southerly extension of subtropical westerly jet streams (STWJ) over North Africa. These narrow and shallow streams of fast-flowing air in the upper troposphere with maximum speed at about 200 Mb level are one of the rain-bearing systems in the region. One can understand from the composite anomaly map in Figure 3(c) and Figure 3(d), that a positive (negative) height anomaly was observed during JJAS (FMAM), which in turn shows suppressed (enhanced) convections persistent in the region.

4.5. Geopotential Height at 850 Mb during the Strong La Niña Years

Note that, long-term mean fields are replicated to compare it with composite mean to have clear pictures of the anomalies of observed fields. The composite mean value of geopotential height at 850 Mb in Figure 4(a) and Figure 4(b)
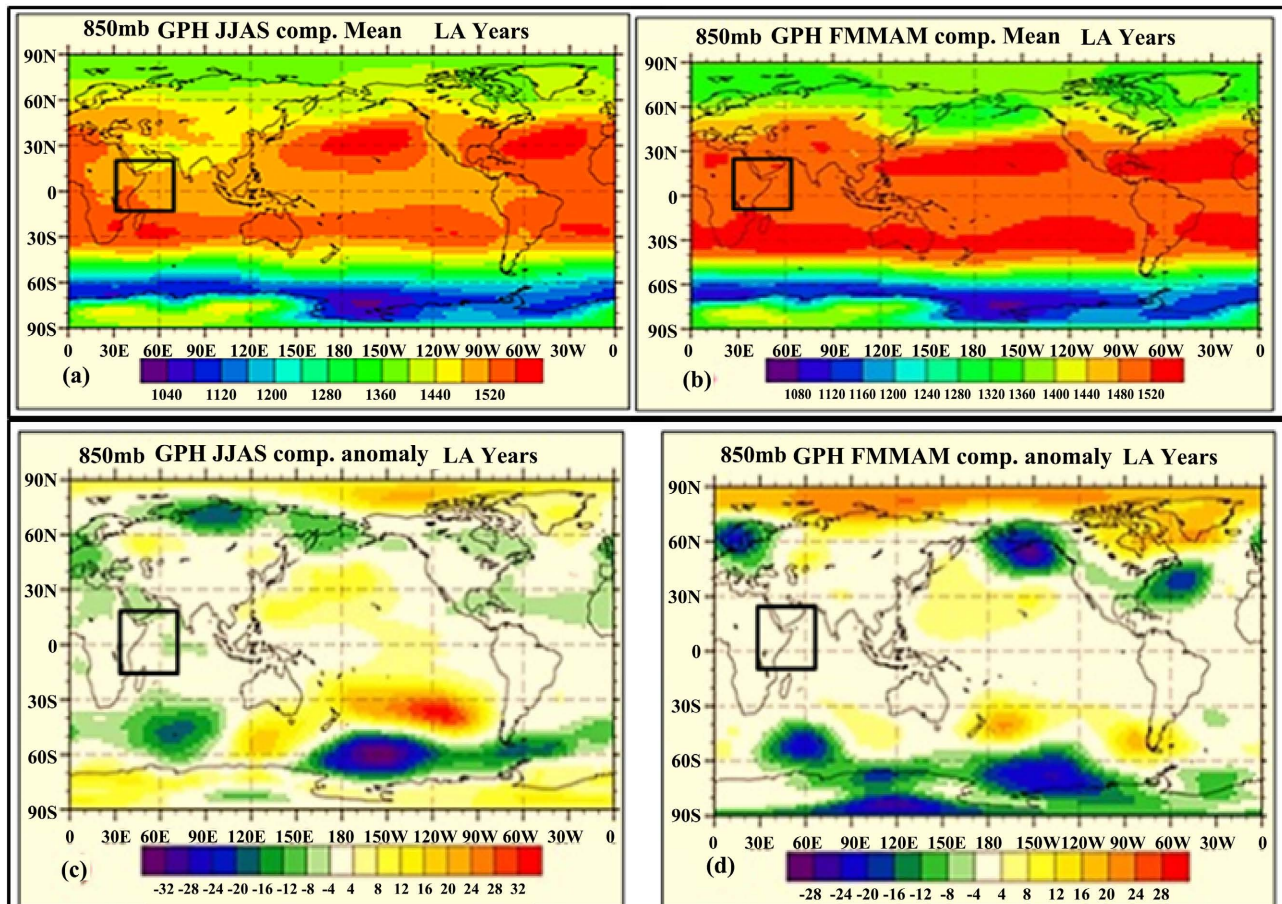

Figure 4. Geopotential heights (850 Mb; m) for (a) JJAS composite mean; (b) FMAM composite Mean; (c) JJAS composite anomaly of six strongest La Niña events; (d) FMAM composite anomaly of six strongest La Niña events.

revealed clear contrast during the dominant rainfall seasons in the region. We can see also, basin-wide intensified composite mean height in the Southern and Northern Pacific Ocean, south India Ocean, and over Australia in FMAM season than JJAS, which might suggest that large scale pressure systems in the tropics had more dominance in regional circulation during FMAM season in La Niña composite years.

850 Mb height anomalies presented in Figure 4(c) and Figure 4(d) show, extra tropical cyclones developed in the southwest Indian Ocean and the South Pacific Ocean. We can see intensified cyclones in number as well as in magnitude in Belg (FMAM) than Kermit (JJAS) season, but nearly similar low height anomaly has been observed in the rim of the eastern Africa region. During boreal summer the central Indian Ocean is characterized by a significant amount of below normal height anomaly which might suggest the warming of the ocean during that time had a role in exacerbating low pressure in the region [7] [28].

The cyclone activities and frequency in the Indian Ocean basin have a crucial impact on the convection activities and moisture advection in the southern as well as northern and central parts of Ethiopia [41]. Supporting this premise, [42] argued that, the cyclones that develop in the southwest Indian Ocean (SWIO) usually travel west then southwest, and finally recurve to the southeast before reaching East Africa and, they further noticed that the cyclone/depression can indirectly affect the weather pattern and condition in Ethiopia.

Fairly opposite 850 Mb geopotential anomalies have been observed during Kiremt season, along the red sea coastline, northwest Indian ocean, and Arabian sea as can be seen from Figure 2(c) and Figure 4(c), which are associated with intensified/repressed low-level pressure during El Niño/La Niña composite year. [22], examined that low/high-pressure anomalies in these regions are associated with excess/deficit rainfall years in central, western, and northwestern regions of Ethiopia. But there is no significant contrast between height anomalies of 200 Mb geopotential for Belg (FMAM) season during El Niño and La Niña composite years as presented in Figure 3(d) and Figure 5(d) respectively, except minor positive anomaly noticed in the northern tip of the country.

4.6. Geopotential Height at 200 Mb during the Strong La Nino Year

The composite anomalies observed in Figure 5(c) and Figure 5(d) during JJAS and FMAM season depict opposite patterns in East Africa especially in the region enclosing Ethiopia (3N - 15N latitude and 32E - 48E longitude), as we can visually inspect from the figures. Also, a strong correlation has been observed between the eastern Pacific Ocean and Eastern Africa height anomaly at 200 Mb pressure level with a positive anomaly in JJAS and negative anomaly in FMAM season as can be seen from Figure 5(c) and Figure 5(e). This informs us factors governing inter-seasonal variability of metrological fields over the region may differ in two seasons.
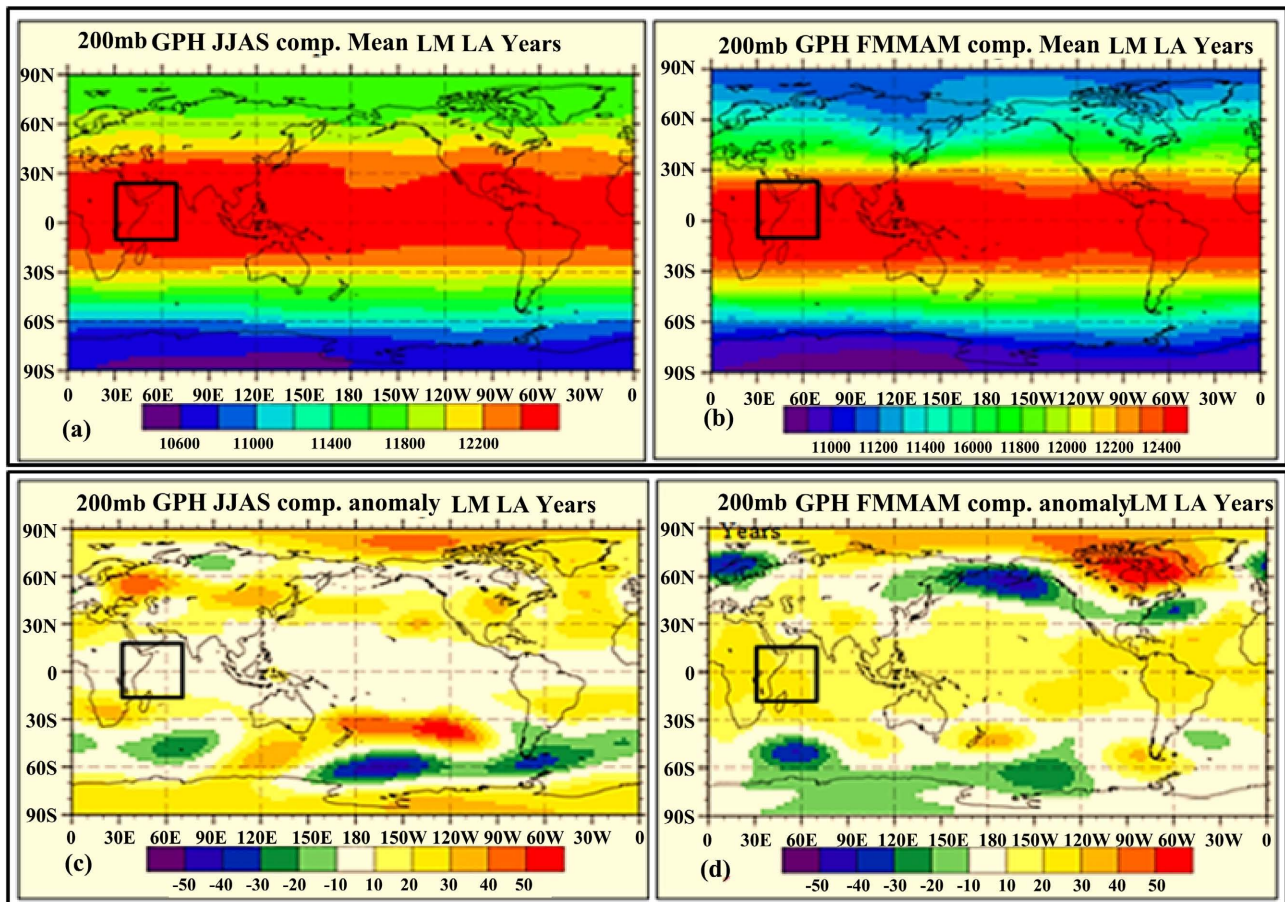
Figure 5. Geopotential heights (200 Mb; m) for (a) JJAS composite mean; (b) FMAM composite Mean; (c) JJAS composite Anomaly of six strongest La Niña events; (d) FMAM composite anomaly of six strongest La Niña events.

A substantial decrease in upper lever height at 200 Mb has been observed in Ethiopia during El Niño composite years (**Figure 3(d)**) when compared to La Niña composite years (**Figure 4(d)**). This asserts that during El Niño years the upper-level divergence may initiate low-level vertical motion and hence enhance convection in the region whereas during La Niña composite years nearly contrasting phenomena have occurred in Belg (FMAM) season. On the other hand, noticeably higher than normal 200 Mb field during strong La Niña composite years over East Africa and central Asia (Tibetan plate) might suggest the strengthening of the subtropical jet stream which can extend its impact to the central and northern part of Ethiopia by suppressing low-level convection [7] [28] [38] [41].

In both cases (850 Mb and 200 Mb) anomalies shown in **Figure 4(c)** & **Figure 4(d)** and **Figure 5(c)** & **Figure 5(d)** below normal height, anomalies are evident in the southwestern Indian ocean but the low is intensified during Belg (FMAM) than Kiremt (JJAS) season. A similar observation was documented by [41] justifying that, Belg rainfall is much more influenced by cyclone activities than Kiremt rainfall, which occurs outside the cyclone season of the Southwest Indian Ocean. [41] also noted that, on a daily basis, rainfall activities during the Belg

period are significantly reduced when a tropical depression is observed in the southwest Indian Ocean.

4.7. Precipitation Rate during the Strong El Niño and La Niña Years

From our previous discussion on rainfall variability in space and time, we noticed that a complex relationship has existed during the ENSO period in a historical record. The rainfall anomaly index analysis used by [9] has revealed this fact. Supporting this, the study carried out by [30] applying harmonic analysis to El Niño Southern Oscillation (ENSO) composite of the 6-months Standardized Precipitation Index (SPI) and rainfall anomaly for the 1900-1996 period has unveiled that ENSO response in East Africa rainfall is region and season dependent, and the influence of El Niño is stronger and opposite than that of La Niña. The composite precipitation rate (mm/day) map presented below in **Figure 6**
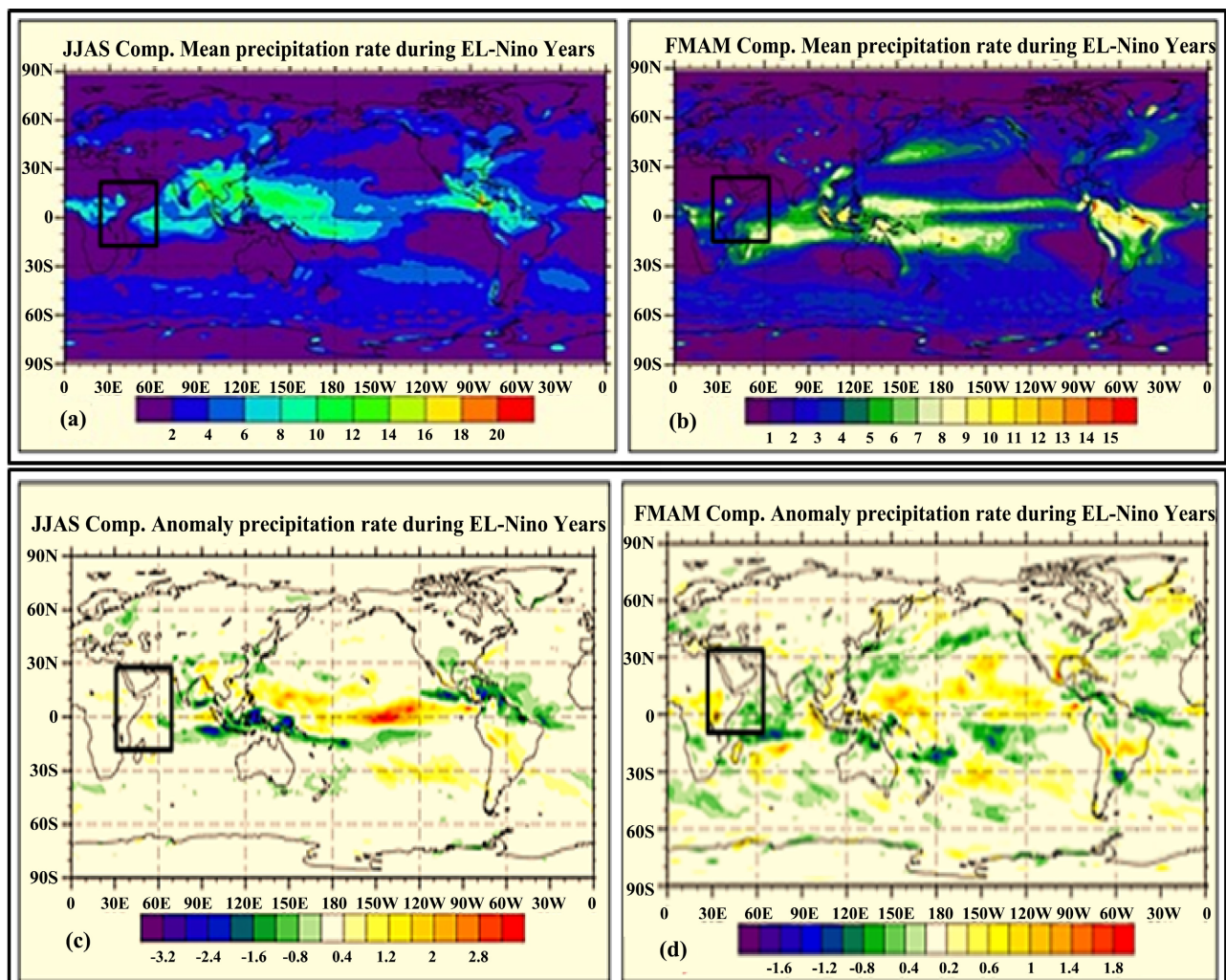

Figure 6. Precipitation rates (mm/day) for (a) composite mean of JJAS for six strongest El Niño events; (b) composite mean of FMAM for six strongest El Niño events; (c) composite anomaly of JJAS six strongest El Niño events; (d) composite anomaly of FMAM six stronges.

and Figure 7(a) & Figure 7(b), show remarkable seasonal variations during El Niño and La-Nina periods respectively. In both cases, the relatively strong precipitation rate has been noticed in equatorial regions between 10S - 10N (not to the scale), this may suggest that tropical regions are most affected by climate anomalies than their extra-topical counterparts.

Composite anomalies during the six strongest El-Nino periods shown in (Figure 6(c), and Figure 6(d)) indicated, suppressed precipitation rate in the southern region of Ethiopia during the JJAS season and an enhanced rate during FMAM season. The same finding was revealed in previous studies [9], using statistical analysis to correlate Nino 3.4 index and standardized precipitation anomaly index in the two rainfall dominate seasons in the region. But, by carefully observing one can see a shift of precipitation rate in the Eastern Africa region and maritime content which is the manifestation of a shift of convection patterns due to ENSO dynamics in the region. Also, one can observe a relatively noticeable contrast in precipitation rate during JJAS than FMAM season in the
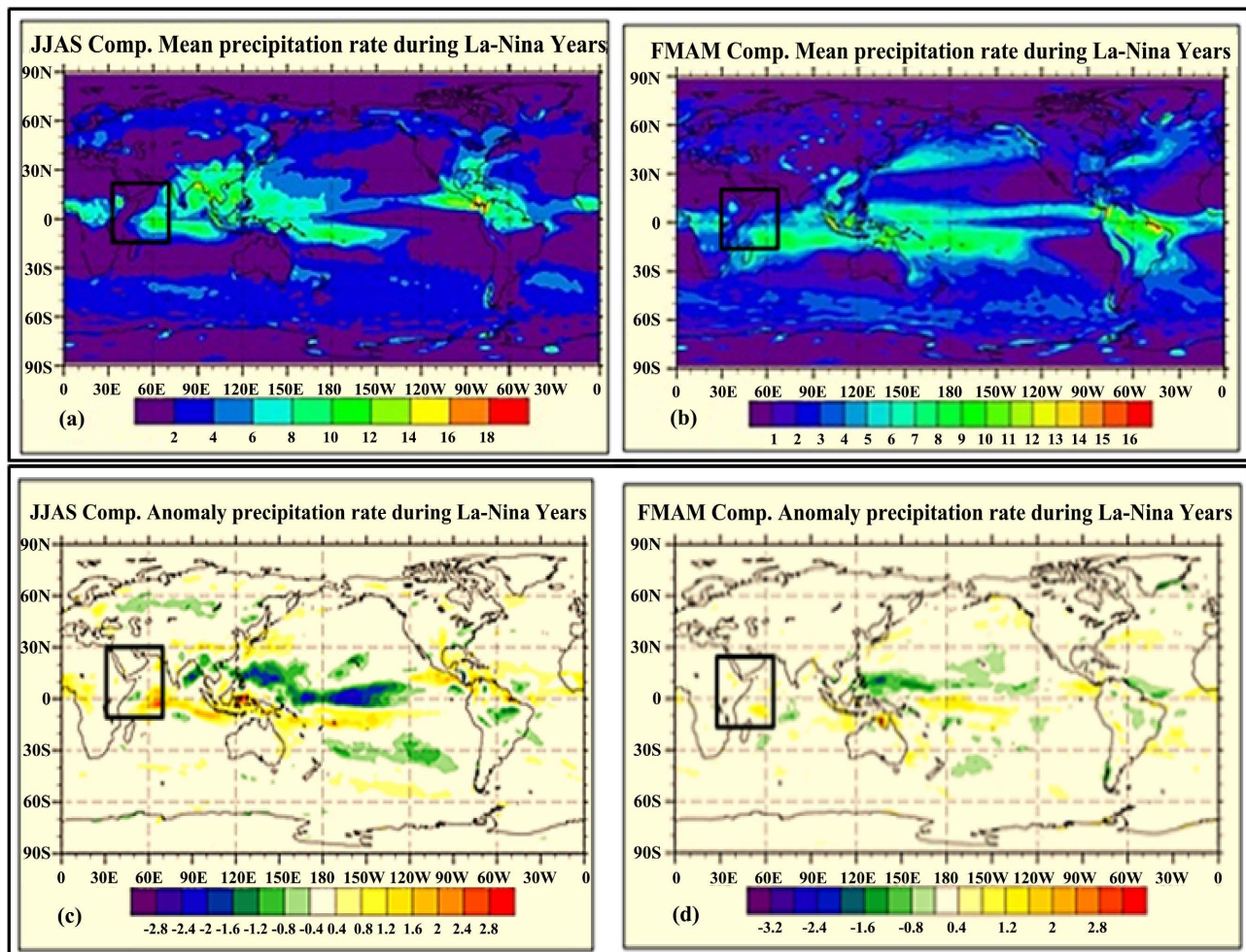

Figure 7. Precipitation rates (mm/day) for (a) composite mean of JJAS for six strongest La Niña events; (b) composite mean of FMAM for six strongest La Niña events; (c) composite anomaly of JJAS six strongest La Niña events; (d) composite anomaly of FMAM six strongest.

central and eastern equatorial Pacific Ocean where the ENSO phenomena are known to prevail [13] [43] [44] [45] [46]. But, **Figure 7(c)**, and d show nearly the opposite precipitation rates in both seasons when compared to the El Niño composite presented in **Figure 6(c)**, and **Figure 6(d)**, however magnificent anomaly is seen during El-Nino episodes than La Niña.

The seasonal and spatial contrast of precipitation rate due to the modulation of ENSO events has a huge impact on vegetation biomass productivity and growth [47] [48]. According to [47], the transition from El Niño to La Niña conditions during the 1997-2000 period had resulted in a severe impact on perception and vegetation biomass over Africa, particularly for East and Southern Africa these teleconnections were very strong. There was a marked contrast in vegetation anomaly patterns during the peak periods of warm (1997/98) and cold (1999/200) ENSO events, which are one of the strongest years selected for our composite analysis.

4.8. Summary and Conclusions

This study examines the composite of geopotential heights at 850 and 200 Mb, and precipitation rates for the six-strong El Niño and La Niña years on rainfall of Kiremt (June to September) and Belg (February to May) seasons of Ethiopia, in the Horn of Africa region.

It has been observed that El Niño and La-Nina response in the HOA regions geopotential height and surface precipitation rate are associated and vary in intensity for two episodes in the opposite manner. Fairly opposite 850 Mb geopotential anomalies have been observed in composite Map during Kiremt season, along the red sea coastline, northwest Indian Ocean, and the Arabian Sea, which are associated with intensified/repressed low-level pressure during El Niño/La Niña composite year. This shows low/high-pressure anomalies in these regions are associated with excess/deficit rainfall years in central, western, and northwestern regions of Ethiopia. Composite anomalies during the six strongest El-Nino periods shown in (**Figure 6(c)**, and **Figure 6(d)** above) indicated, suppressed precipitation rate in the southern region of Ethiopia during the JJAS season and an enhanced rate during FMAM season. The same finding was revealed in previous studies [9], using statistical analysis to correlate Nino 3.4 index and standardized precipitation anomaly index in the two rainfall dominate seasons in the region.

The composite analysis approach employed in this study provides insights into tropical large-scale dynamics (ENSO) association with regional climate variability triggered by upper and lower level atmospheric circulation patterns represented by geopotential height anomalies. However, further studies integrating numerical modeling and intense observational analysis including different variables and spatial extents (horizontal as well as vertical) should be done to fully understand the phenomena controlling climate fluctuation in the region.

This study has focused only on two rainy seasons in Ethiopia, represented by a

composite of geopotential height at 850 and 200 Mb, and surface precipitation rate (mm/day) for the six strongest El Niño and La Niña events. It has been observed that El Niño and La-Nino response in the HOA regions geopotential height and surface precipitation rate are associated and varies in intensity for two episodes in the opposite manner. Fairly opposite 850 Mb geopotential anomalies have been observed in composite Map during Kiremt season, along the red sea coastline, northwest Indian Ocean, and the Arabian Sea, which are associated with intensified/repressed low-level pressure during El Niño/La Niña composite year. This shows low/high-pressure anomalies in these regions are associated with excess/deficit rainfall years in central, western, and northwestern regions of Ethiopia. Composite anomalies during the six strongest El-Nino periods shown in (Figure 6(c), and Figure 6(d) above) indicated, suppressed precipitation rate in the southern region of Ethiopia during the JJAS season and an enhanced rate during FMAM season. The same finding was revealed in previous studies [9], using statistical analysis to correlate Nino 3.4 index and standardized precipitation anomaly index in the two rainfall dominate seasons in the region.

Acknowledgements

Conflicts of Interest

The authors declare no conflicts of interest regarding the publication of this paper.

References

[1] Daron, D.J.D. (2018) Regional Climate Messages for East Africa. International Development Research Centre. Ottawa, Canada.

[2] Riddle, E.E. and Cook, K.H. (2008) Abrupt Rainfall Transitions over the Greater Horn of Africa: Observations and Regional Model Simulations. *Journal of Geophysical Research*: *Atmospheres*, **113**, Article ID: D15109.
https://doi.org/10.1029/2007JD009202

[3] Meehl, G.A., Hu, A., Arblaster, J.M., Fasullo, J. and Trenberth, K.E. (2013) Externally Forced and Internally Generated Decadal Climate Variability Associated with the Interdecadal Pacific Oscillation. *Journal of Climate*, **26**, 7298-7310.
https://doi.org/10.1175/JCLI-D-12-00548.1

[4] Meehl, G.A., Goddard, L., Murphy, J., Stouffer, R.J., Boer, G., Danabasoglu, G. and Stockdale, T. (2009) Decadal Prediction: Can It Be Skillful? *Bulletin of the American Meteorological Society*, **90**, 1467-1486. https://doi.org/10.1175/2009BAMS2778.1

[5] Keenlyside, N.S. and Ba, J. (2010) Prospects for Decadal Climate Prediction. *Wiley Interdisciplinary Reviews*: *Climate Change*, **1**, 627-635.
https://doi.org/10.1002/wcc.69

[6] Jury, M.R. (2010) Ethiopian Decadal Climate Variability. *Theoretical and Applied*

Climatology, **101**, 29-40. https://doi.org/10.1007/s00704-009-0200-3

[7] LaJoie, M.R. (2006) The Impacts of Climate Variations on Military Operations in the Horn of Africa. Master's Thesis, Naval Postgraduate School, Monterey, USA.

[8] Segele, Z.T., Lamb, P.J. and Leslie, L.M. (2009) Seasonal-to-Interannual Variability of Ethiopia/Horn of Africa Monsoon. Part I: Associations of Wavelet-Filtered Large-Scale Atmospheric Circulation and Global Sea Surface Temperature. *Journal of Climate*, **22**, 3396-3421. https://doi.org/10.1175/2008JCLI2859.1

[9] Gunta, S., Manjunatha, B. and Bhat, H.G. (2019) Monthly to Inter-Decadal Rainfall Variability of the Southern Regional State of Ethiopia, Links with El Niño-Southern Oscillation. *Global Journal of Science Frontier Research*: *H*, **19**, 13-31.

[10] Camberlin, P., Janicot, S. and Poccard, I. (2001) Seasonality and Atmospheric Dynamics of the Teleconnection between African Rainfall and Tropical Sea-Surface Temperature: Atlantic vs. ENSO. *International Journal of Climatology*, **21**, 973-1005. https://doi.org/10.1002/joc.673

[11] Camberlin, P. and Philippon, N. (2002) The East African March-May Rainy Season: Associated Atmospheric Dynamics and Predictability over the 1968-97 Period. *Journal of Climate*, **15**, 1002-1019. https://doi.org/10.1175/1520-0442(2002)015<1002:TEAMMR>2.0.CO;2

[12] Camberlin, P. (1997) Rainfall Anomalies in the Source Region of the Nile and Their Connection with the Indian Summer Monsoon. *Journal of Climate*, **10**, 1380-1392. https://doi.org/10.1175/1520-0442(1997)010<1380:RAITSR>2.0.CO;2

[13] Endris, H.S., Lennard, C., Hewitson, B., Dosio, A., Nikulin, G. and Artan, G.A. (2019) Future Changes in Rainfall Associated with ENSO, IOD and Changes in the Mean State over Eastern Africa. *Climate Dynamics*, **52**, 2029-2053. https://doi.org/10.1007/s00382-018-4239-7

[14] Seleshi, Y. and Demaree, G.R. (1995) Rainfall Variability in the Ethiopian and Eritrean Highlands and Its Links with the Southern Oscillation Index. *Journal of Biogeography*, **22**, 945-952. https://doi.org/10.2307/2845995

[15] Dimri, A.P. (2013) Relationship between ENSO Phases with Northwest India Winter Precipitation. *International Journal of Climatology*, **33**, 1917-1923. https://doi.org/10.1002/joc.3559

[16] Korecha, D. and Barnston, A.G. (2007) Predictability of June-September Rainfall in Ethiopia. *Monthly Weather Review*, **135**, 628-650. https://doi.org/10.1175/MWR3304.1

[17] Bahaga, T.K., Fink, A.H. and Knippertz, P. (2019) Revisiting Interannual to Decadal Teleconnections Influencing Seasonal Rainfall in the Greater Horn of Africa during the 20th Century. *International Journal of Climatology*, **39**, 2765-2785. https://doi.org/10.1002/joc.5986

[18] Ngarukiyimana, J.P., Fu, Y., Yang, Y., Ogwang, B.A., Ongoma, V. and Ntwali, D. (2018) Dominant Atmospheric Circulation Patterns Associated with Abnormal Rainfall Events over Rwanda, East Africa. *International Journal of Climatology*, **38**, 187-202. https://doi.org/10.1002/joc.5169

[19] Okoola, R.E. (1999) A Diagnostic Study of the Eastern Africa Monsoon Circulation during the Northern Hemisphere Spring Season. *International Journal of Climatology*, **19**, 143-168. https://doi.org/10.1002/(SICI)1097-0088(199902)19:2<143::AID-JOC342>3.0.CO;2-U

[20] Ogwang, B.A., Chen, H., Tan, G., Ongoma, V. and Ntwali, D. (2015) Diagnosis of East African Climate and the Circulation Mechanisms Associated with Extreme Wet and Dry Events: A Study Based on RegCM4. *Arabian Journal of Geosciences*, **8**, 10255-10265. https://doi.org/10.1007/s12517-015-1949-6

[21] Zeleke, T., Giorgi, F., Mengistu Tsidu, G. and Diro, G.T. (2013) Spatial and Temporal Variability of Summer Rainfall over Ethiopia from Observations and a Regional Climate Model Experiment. *Theoretical and Applied Climatology*, **111**, 665-681. https://doi.org/10.1007/s00704-012-0700-4

[22] Diro, G.T., Grimes, D.I.F. and Black, E. (2011) Teleconnections between Ethiopian Summer Rainfall and Sea Surface Temperature: Part I-Observation and Modelling. *Climate Dynamics*, **37**, 103-119. https://doi.org/10.1007/s00382-010-0837-8

[23] Diro, G.T., Grimes, D.I.F. and Black, E. (2011) Large Scale Features Affecting Ethiopian Rainfall. In: Williams, C. and Kniveton, D., Eds., *African Climate and Climate Change*, Springer, Dordrecht, 13-50. https://doi.org/10.1007/978-90-481-3842-5_2

[24] Dinku, T., Funk, C., Peterson, P., Maidment, R., Tadesse, T., Gadain, H. and Ceccato, P. (2018) Validation of the CHIRPS Satellite Rainfall Estimates over Eastern Africa. *Quarterly Journal of the Royal Meteorological Society*, **144**, 292-312. https://doi.org/10.1002/qj.3244

[25] Peel, M.C., Finlayson, B.L. and McMahon, T.A. (2007) Updated World Map of the Köppen-Geiger Climate Classification. *Hydrology and Earth System Sciences*, **11**, 1633-1644. https://doi.org/10.5194/hess-11-1633-2007

[26] Segele, Z.T., Lamb, P.J. and Leslie, L.M. (2009) Large-Scale Atmospheric Circulation and Global Sea Surface Temperature Associations with Horn of Africa June-September Rainfall. *International Journal of Climatology*, **29**, 1075-1100. https://doi.org/10.1002/joc.1751

[27] Lyon, B. (2014) Seasonal Drought in the Greater Horn of Africa and Its Recent Increase during the March-May Long Rains. *Journal of Climate*, **27**, 7953-7975. https://doi.org/10.1175/JCLI-D-13-00459.1

[28] Vorhees, D.C. (2006) The Impacts of Global Scale Climate Variations on Southwest Asia. Naval Postgraduate School, Monterey.

[29] Kalnay, E., Kanamitsu, M., Kistler, R., Collins, W., Deaven, D. and Gandin, L. (1996) The NCEP/NCAR 40-Year Reanalysis Project. *Bulletin of the American Meteorological Society*, **77**, 437-472. https://doi.org/10.1175/1520-0477(1996)077<0437:TNYRP>2.0.CO;2

[30] Ntale, H.K. and Gan, T.Y. (2004) East African Rainfall Anomaly Patterns in Association with El Nino/Southern Oscillation. *Journal of Hydrologic Engineering*, **9**, 257-268. https://doi.org/10.1061/(ASCE)1084-0699(2004)9:4(257)

[31] Folland, C.K. (1983) Regional-Scale International Variability of Climate. A North-West European Perspective. *Meteorological Magazine*, **112**, 163-183.

[32] Dezfuli, A.K. and Nicholson, S.E. (2011) A Note on Long-Term Variations of the African Easterly Jet. *International Journal of Climatology*, **31**, 2049-2054. https://doi.org/10.1002/joc.2209

[33] Sultan, B. and Janicot, S. (2003) The West African Monsoon Dynamics. Part II: The "Preonset" and "Onset" of the Summer Monsoon. *Journal of Climate*, **16**, 3407-3427. https://doi.org/10.1175/1520-0442(2003)016<3407:TWAMDP>2.0.CO;2

[34] Okoola, R.E. (1999) Midtropospheric Circulation Patterns Are Associated with Extremely Dry and Wet Episodes over Equatorial Eastern Africa during the Northern Hemisphere Spring. *Journal of Applied Meteorology and Climatology*, **38**, 1161-1169. https://doi.org/10.1175/1520-0450(1999)038<1161:MCPAWE>2.0.CO;2

[35] Hastenrath, S. (2001) Variations of East African Climate during the Past Two Centuries. *Climatic Change*, **50**, 209-217. https://doi.org/10.1023/A:1010678111442

[36] Blackmon, M.L. (1976) A Climatological Spectral Study of the 500 Mb Geopotential

Height of the Northern Hemisphere. *Journal of the Atmospheric Sciences*, **33**, 1607-1623. https://doi.org/10.1175/1520-0469(1976)033<1607:ACSSOT>2.0.CO;2

[37] Thompson, D.W. and Wallace, J.M. (1998) The Arctic Oscillation Signature in the Wintertime Geopotential Height and Temperature Fields. *Geophysical Research Letters*, **25**, 1297-1300. https://doi.org/10.1029/98GL00950

[38] Camberlin, P. and Okoola, R.E. (2003) The Onset and Cessation of the "Long Rains" in Eastern Africa and Their Interannual Variability. *Theoretical and Applied Climatology*, **75**, 43-54. https://doi.org/10.1007/s00704-002-0721-5

[39] Vizy, E.K. and Cook, K.H. (2003) Connections between the Summer East African and Indian Rainfall Regimes. *Journal of Geophysical Research*: *Atmospheres*, **108**, Article No. 4510. https://doi.org/10.1029/2003JD003452

[40] Gissila, T., Black, E., Grimes, D.I.F. and Slingo, J.M. (2004) Seasonal Forecasting of the Ethiopian Summer Rains. *International Journal of Climatology*, **24**, 1345-1358. https://doi.org/10.1002/joc.1078

[41] Segele, Z.T. and Lamb, P.J. (2005) Characterization and Variability of Kiremt Rainy Season over Ethiopia. *Meteorology and Atmospheric Physics*, **89**, 153-180. https://doi.org/10.1007/s00703-005-0127-x

[42] Shanko, D. and Camberlin, P. (1998) The Effects of the Southwest Indian Ocean Tropical Cyclones on Ethiopian Drought. *International Journal of Climatology*, **18**, 1373-1388. https://doi.org/10.1002/(SICI)1097-0088(1998100)18:12<1373::AID-JOC313>3.0.CO;2-K

[43] Wang, H.J., Zhang, R.H., Cole, J. and Chavez, F. (1999) El Niño and the Related Phenomenon Southern Oscillation (ENSO): The Largest Signal in Interannual Climate Variation. *Proceedings of the National Academy of Sciences of the United States of America*, **96**, 11071-11072. https://doi.org/10.1073/pnas.96.20.11071

[44] Lau, K.M. and Shen, S. (1988) on the Dynamics of Intraseasonal Oscillations and ENSO. *Journal of Atmospheric Sciences*, **45**, 1781-1797. https://doi.org/10.1175/1520-0469(1988)045<1781:OTDOIO>2.0.CO;2

[45] Indeje, M., Semazzi, F.H. and Ogallo, L.J. (2000) ENSO Signals in East African Rainfall Seasons. *International Journal of Climatology*, **20**, 19-46. https://doi.org/10.1002/(SICI)1097-0088(200001)20:1<19::AID-JOC449>3.0.CO;2-0

[46] Wolter, K. and Timlin, M.S. (2011) El Ni No/Southern Oscillation Behavior since 1871 as Diagnosed in an Extended Multivariate ENSO Index (MEI. Ext). *International Journal of Climatology*, **1087**, 1074-1087. https://doi.org/10.1002/joc.2336

[47] Anyamba, A., Tucker, C.J. and Mahoney, R. (2002) from El Niño to La Niña: Vegetation Response Patterns over East and Southern Africa during the 1997-2000 Period. *Journal of Climate*, **15**, 3096-3103. https://doi.org/10.1175/1520-0442(2002)015<3096:FENOTL>2.0.CO;2

[48] Tshiabukole, K., Khonde, P., Muku, M., Vumilia, K., Lunekua, K. and Kankolongo, M. (2016) Influence of Climate Variability on Seasonal Rainfall Patterns in South-Western DR Congo. *Open Access Library Journal*, **3**, Article ID: e2952. https://doi.org/10.4236/oalib.1102952